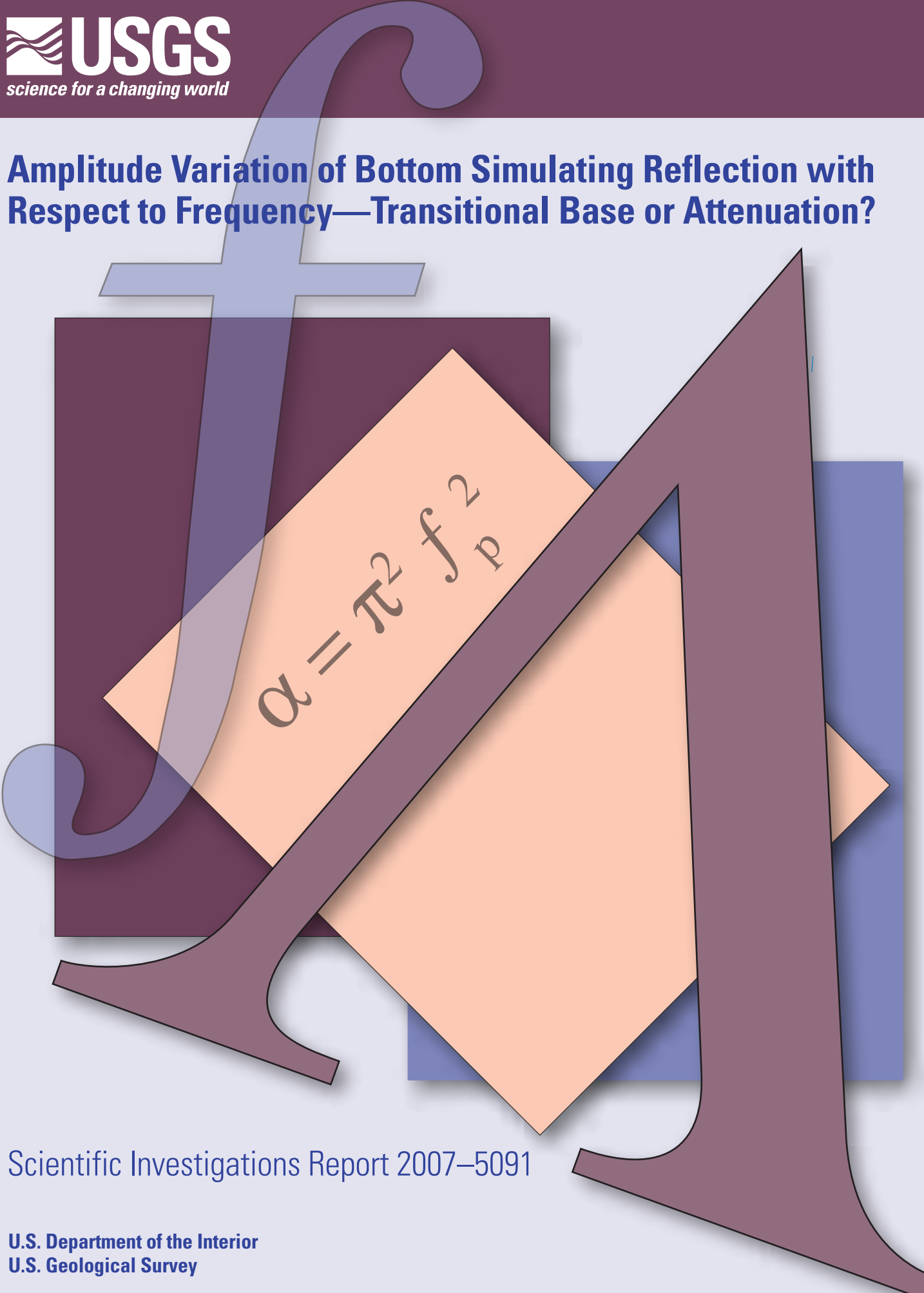![USGS logo] USGS
science for a changing world

Amplitude Variation of Bottom Simulating Reflection with Respect to Frequency—Transitional Base or Attenuation?

$$\alpha = \pi^2 f^2_p$$

Scientific Investigations Report 2007–5091

U.S. Department of the Interior
U.S. Geological Survey

Amplitude Variation of Bottom Simulating Reflection with Respect to Frequency—Transitional Base or Attenuation?

By Myung W. Lee

Scientific Investigations Report 2007–5091

U.S. Department of the Interior
DIRK KEMPTHORNE, Secretary

U.S. Geological Survey
Mark D. Myers, Director

U.S. Geological Survey, Reston, Virginia: 2007

Contents

Figures

Amplitude Variation of Bottom Simulating Reflection with Respect to Frequency—Transitional Base or Attenuation?

By Myung W. Lee

Abstract

The amplitude of a bottom simulating reflection (BSR), which occurs near the phase boundary between gas hydrate-bearing sediments and underlying gas-filled sediments, strongly depends on the frequency content of a seismic signal, as well as the impedance contrast across the phase boundary. A strong-amplitude BSR, detectable in a conventional seismic profile, is a good indicator of the presence of free gas beneath the phase boundary. However, the BSR as observed in low-frequency multichannel seismic data is generally difficult to identify in high-frequency, single-channel seismic data.

To investigate the frequency dependence of BSR amplitudes, single-channel seismic data acquired with an air gun source at Blake Ridge, which is located off the shore of South Carolina, were analyzed in the frequency range of 10–240 Hz. The frequency-dependent impedance contrast caused by the velocity dispersion in partially gas saturated sediments is important to accurately analyze BSR amplitude. Analysis indicates that seismic attenuation of gas hydrate-bearing sediments, velocity dispersion, and a transitional base all contribute to the frequency-dependent BSR amplitude variation in the frequency range of 10–500 Hz. When velocity dispersion is incorporated into the BSR amplitude analysis, the frequency-dependent BSR amplitude at Blake Ridge can be explained with gas hydrate-bearing sediments having a quality factor of about 250 and a transitional base with a thickness of about 1 meter.

Introduction

Gas hydrates, or clathrates, are ice-like crystalline solids composed of water molecules surrounding a gas molecule. The importance of gas hydrates as a potential energy source, as a greenhouse gas, and as a hazard for sea floor stability has been investigated (Kvenvolden, 1988; Dillon and others, 1991; Paull and others, 1991; Collett, 1996).

Gas hydrates form at appropriate temperature and pressure conditions when water is saturated with gas, and they are stable within the upper several hundred meters of sediments below sea floor (Claypool and Kaplan, 1974). The presence of methane gas hydrates in ocean sediments has generally been inferred from the bottom simulating reflection (BSR) in seismic profiles (Markl and others, 1970; Shipley and others, 1979). The BSR simulates the surface of sea floor because the base of hydrate phase stability or phase boundary parallels the sea floor.

Hyndman and Spencer (1992) and Hyndman and Davis (1992) presented a model in which a BSR is generated by impedance contrast between sediments that have about 30 percent of the pore space filled with gas hydrate and the underlying sediments containing neither hydrate nor seismically detectable free gas. Their conclusion is based on an analysis of the reflection coefficient, vertical-incidence waveform, amplitude-versus-offset, and velocity structure. The best fit model for the seismic data is gas hydrate-bearing sediments (GHBS) having a sharp base and transitional top.

Except in the Hyndman and Spencer (1992) model, however, the high-amplitude BSR is generally interpreted as a reflection from a boundary between GHBS and underlying gas-filled sediments near the phase boundary (Shipley and others, 1979; Andreassen and Berteussen, 1990; Miller and others, 1991; Dillon and others, 1994). The Ocean Drilling Program (ODP) Leg 164, Sites 995 and 997 (Shipboard Scientific Party, 1996), proved the existence of free gas beneath the GHBS and confirmed that the BSR is caused by a marked impedance contrast across the methane hydrate phase boundary.

Lee and others (1994) demonstrated that the amplitude of BSR depends largely on the frequency content of the source signal. When a very high frequency seismic source is used, the continuous looking BSR in the low-frequency, multichannel seismic data appears as discontinuous and weak reflections (Lee and others, 1994; Gettrust and others, 1999). Chapman and others (2002) attributed the frequency-dependent amplitude of BSR, observed in the offshore of western Canada, to a transitional layer 4 to 8 m thick.

In order to examine the BSR amplitude characteristics with respect to the frequency content, single-channel seismic data from the Blake Ridge area acquired with an air gun source were analyzed. Two predictive models, one having a transitional layer at the base of GHBS and one with seismic attenuation within GHBS, were analyzed in terms of BSR amplitude and frequency.

Theory and Models

Velocity of Partially Gas Saturated Sediments

Because the BSR occurs at the impedance contrast between GHBS and partially gas saturated sediments (PGSS), it is important to examine the behavior of *P*-wave velocities of PGSS with respect to frequency. The *P*-wave velocity of partially gas saturated sediments with respect to frequency can be predicted using a model proposed by White (1975). The essence of this model is that it includes coupling between fluid-flow waves and seismic body waves; also, it assumes that the medium consists of concentric spheres, where the outer part of the sphere is water saturated and the inner part is gas saturated. One important parameter of the model is the radius of the outer spherical shell, indicated as parameter *b*, which is a free parameter that can be adjusted to fit the measured dispersion relation. The radius of the inner sphere depends on the gas saturation and parameter *b*. For typical seismic frequencies, the White (1975) model predicts large *P*-wave dispersion when free gas saturation is low.

Figure 1 shows calculated *P*-wave velocities for the partially gas saturated sediments (PGSS), with the following parameters: porosity (ϕ), 0.55; clay volume content (C_v), 0.4; differential pressure (*p*), 6 MPa; gas saturation (S_g), 0.04; *b* = 3 cm; and permeability, 100 mD. The bulk and shear moduli of dry sediments were computed using the modified Biot-Gassmann theory proposed by Lee (2002).

The *P*-wave velocity at low frequencies, < 30 Hz, is 1.1 km/s, whereas at high frequencies, > 200 Hz, it is about 1.5 km/s. At logging frequencies in the range of 10 kHz, the *P*-wave velocity is about 1.6 km/s, which agrees with the well log velocities acquired at the Blake Ridge (Guerin and others, 1999). The transition frequency between high and low velocities depends on parameter *b*: as *b* decreases, the transition frequency increases. Because the *P*-wave velocity varies with frequency, the impedance contrast also varies with frequency.

Figure 1 also shows reflection coefficients with respect to frequency, assuming that the *P*-wave velocity of upper GHBS is 1.9 km/s. The reflection coefficient is about 0.3 at frequencies that are less than about 20 Hz, and then decreases as the frequency increases. The reflection coefficient is less than 0.1 at frequencies greater than about 400 Hz. This implies that without any additional factors controlling the BSR amplitude with frequency, velocity dispersion alone decreases the BSR amplitude by about 3 times.

Transitional Base Model

Reflection characteristics from the transitional layer are given by Justice and Zuba (1986). To analyze BSR amplitudes, a symmetrical Ricker wavelet is used. A second-order transition
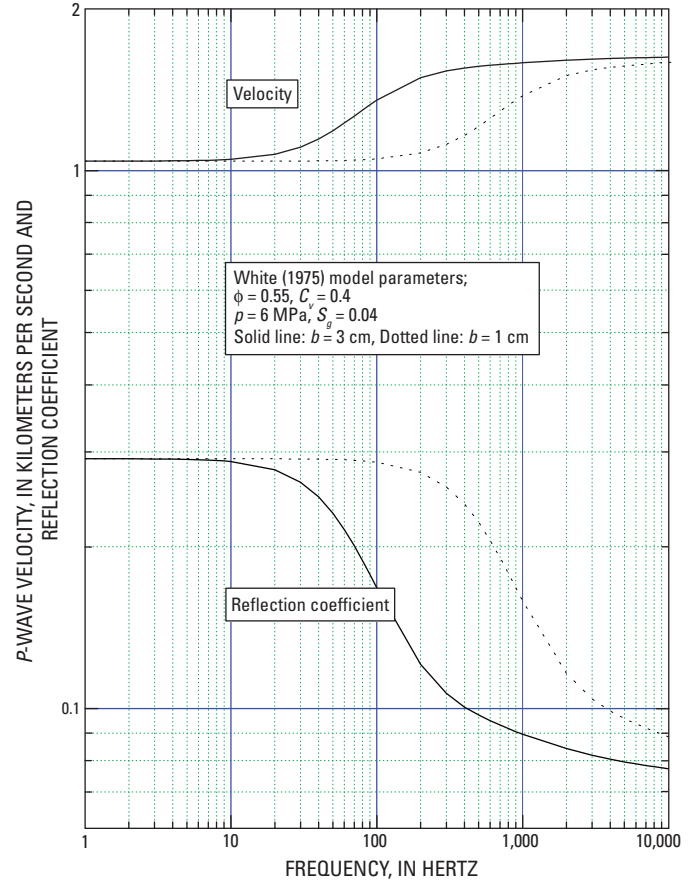
Figure 1. Relationship among *P*-wave velocity, reflection coefficient, and frequency. The bulk and shear moduli of dry rock for this model are 0.7 GPa and 0.5 GPa, respectively, which were calculated using the modified Biot-Gassmann theory proposed by Lee (2002). ϕ, porosity; C_v, clay volume; *p*, differential pressure; GPa, gigapascal; S_g, gas saturation; *b*, adjustable parameter.

zone, which is defined in such a way that the starting and ending velocities of the transition layer are equal to the upper- and lower-layer velocities respectively, is considered. The detailed reflection characteristics from a second-order transitional layer using the Ricker wavelet are given in the Appendix.

The reflected waveform ($S(t)$) from the transitional boundary is given by

$$S(t) = \frac{\ln(V_1/V_0)}{2T} \int r(\tau)d\tau \qquad (1)$$

where

$\quad V_0 \quad$ is the velocity at the top of the transition zone,

$\quad V_1 \quad$ is the velocity at the bottom of the transition zone,

and

$\quad T \quad$ is the width of the transition zone in two-way time.

By integration of equation 1, the maximum amplitude expected from the transitional layer can be derived. Three different cases are considered:

1. The duration of the wavelet is similar to or longer than the transitional layer thickness. In this case, the extreme occurs at $t = -T/2$ and the extreme is given by

$$A_{max} = cG(T/2) = ce^{-\alpha(T/2)^2} \qquad (2)$$

where $c = \ln(V_1/V_0)$.

2. The duration of the input wavelet is much shorter than the transition thickness. In this case, there is no interference between the top and bottom reflections. Therefore, two extreme amplitude points exist, as given by the following equation:

$$A_{max} = \frac{c}{T}\sqrt{\frac{1}{2\alpha}}e^{-1/2} \qquad (3)$$

3. If the duration of the input wavelet is between case 1 and case 2, there is no simple analytic solution.

In order to investigate the BSR amplitude with respect to the input frequency, a simple BSR model, qualitatively similar to the observed BSR at the Blake Ridge, was generated, as shown in figure 2. The model consists of (1) a section of GHBS about 150 m thick with a variable second-order transitional base; (2) velocity increased for the GHBS from mean values of 2.05 km/s at depth of 150 m to 2.25 km/s at
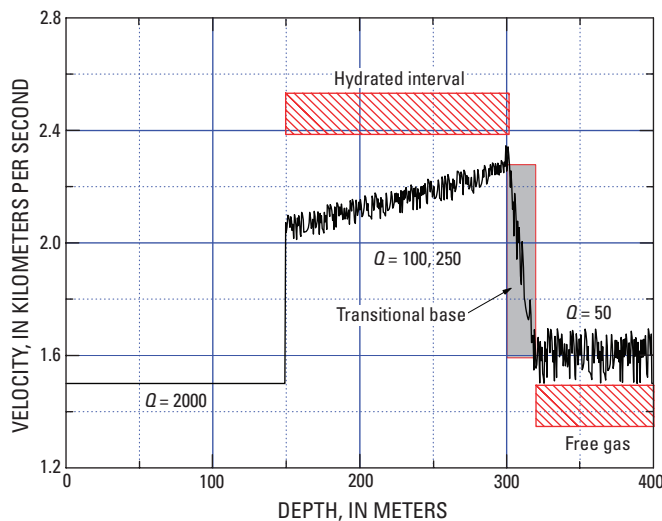
Figure 2. Seismic model for bottom simulating reflections (BSR). Model consists of gas hydrate-bearing sediments (GHBS) having a linearly increasing velocity with depth and a transitional base at the bottom of GHBS and underlying gas-filled sediments having a constant velocity. High-frequency random velocity fluctuations are superimposed on the basic BSR model and are ±0.1 km/s for gas hydrate-bearing sediment and ±0.2 km/s for gas-filled sediments. Q, quality factor.
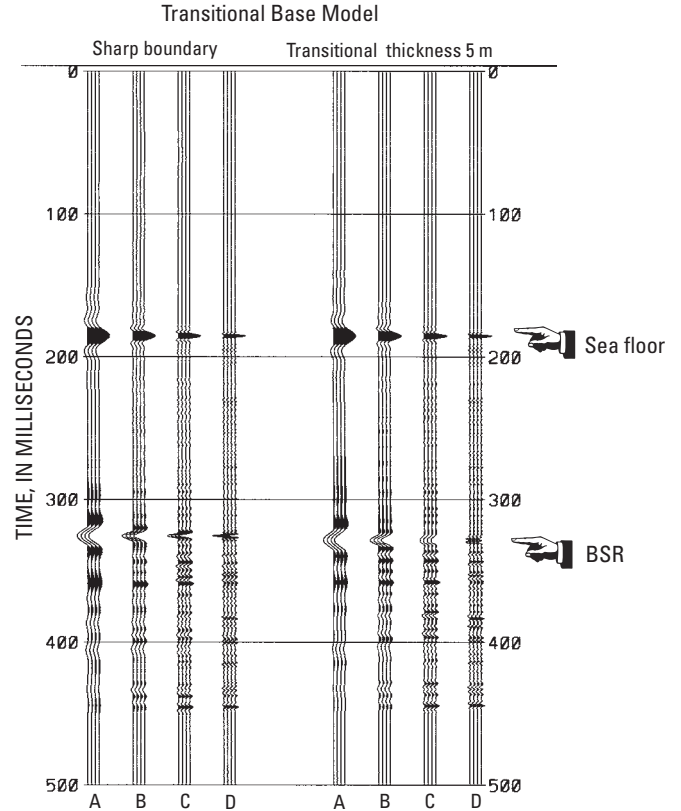
Figure 3. Synthetic bottom simulating reflection (BSR) seismograms with different frequencies using a transitional base model. The left four plots are synthetic waveforms from a sharp boundary, and the right four plots are those from a 5-m thick transition layer. *A*, 10–60 Hz; *B*, 10–120 Hz; *C*, 10–240 Hz; *D*, 10–480 Hz.

depth of 300 m; and (3) a PGSS section with a velocity of 1.6 km/s underlying the transitional layer. To mimic variable velocities of GHBS and PGSS, random velocity fluctuations of 0.1 km/s and 0.2 km/s are superimposed on GHBS and PGSS, respectively.

Figure 3 shows synthetic seismograms for a sharp boundary and for a second-order transitional layer having 5 m thickness. The frequency contents of the synthetics are 10–60 Hz, 10–120 Hz, 10–240 Hz, and 10–480 Hz for A, B, C, and D respectively. For reflections from a sharp boundary (fig. 3), the BSR maintains the same waveform and amplitude except narrowing of the waveform with increasing frequency content. The basic trough waveform can be readily identified irrespective of the frequency content. However, the characteristics of a BSR from the transitional layer are more complicated: as the frequency content increases, the amplitudes of the BSR decrease and it becomes more difficult to identify the BSR. Because the only difference between the two models is the characteristics of the reflector at the BSR level, other reflections are almost identical for each frequency band (fig. 3). Note that a small difference does exist because the interbed multiple contributions are slightly different.

Attenuation Model

Another mechanism of reducing amplitude of the BSR with respect to frequency is seismic attenuation. Two different attenuation models (quality factors of 100 and 250 for GHBS) are shown in figure 2, and the synthetic seismograms including attenuation are shown in figure 4. In this case, the amplitudes of BSR decrease as the frequency content increases, like the model for the transitional layer (fig. 3), but the basic waveforms are almost identical irrespective of the frequency content. The broadened waveform of the BSR observed for the transitional model is not apparent in the attenuation model.

BSR Amplitude from Real Seismic Data

Single-channel, vertical-incidence reflection data acquired at Blake Ridge using an air gun source are shown in figure 5 for three different frequency bands: 10–60 Hz, 10–120 Hz, 10–240 Hz. Qualitatively, the amplitude ratio of the water bottom reflection to BSR decreases as the frequency content increases, as demonstrated in the BSR model study shown in figure 4.
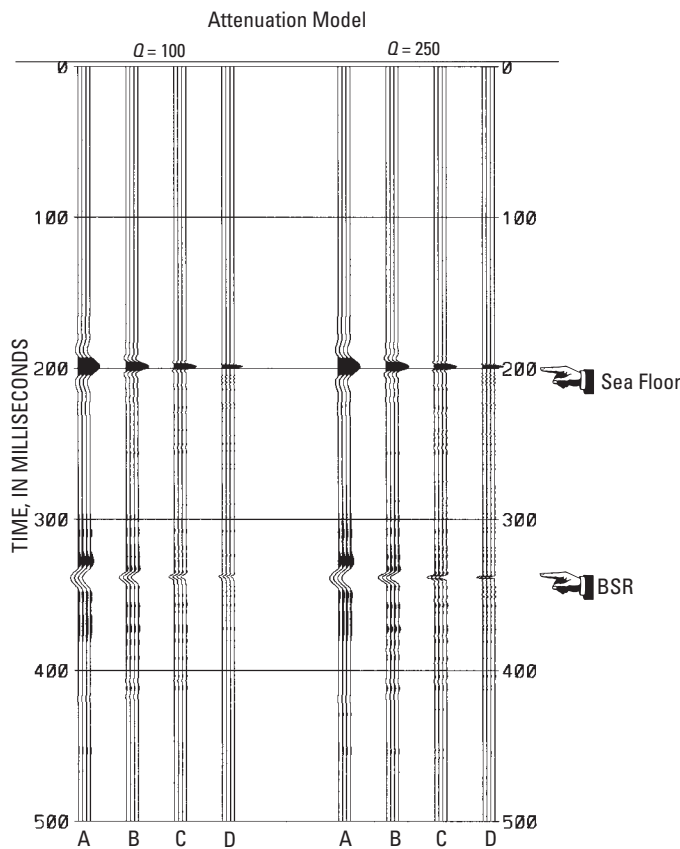
Figure 4.   Synthetic bottom simulating reflection (BSR) seismograms with different frequencies using attenuation models having a sharp boundary. The left four plots are synthetic waveforms with Q = 100, and the right four plots are those with Q = 250. *A,* 10–60 Hz; *B,* 10–120 Hz; *C,* 10–240 Hz; *D,* 10–480 Hz. *Q,* quality factor.

Both a root-mean-square (RMS) amplitude and a trough-peak amplitude within a 20-ms to 40-ms window were measured in order to quantify the amplitude variation of BSR with respect to the frequency content. For the frequency ranges of 10 to 60 Hz, 10 to 120 Hz, and 10 to 240 Hz, the ratios of RMS amplitude of water bottom reflection to the BSR reflection are 1.09 ± 0.24, 0.79 ± 0.19, and 0.6229 ± 0.15; and those when trough-peak amplitude is used are 1.07 ± 0.28, 0.63 ± 0.18, and 0.51 ± 0.16 for 10–60 Hz. As the dominant frequency changes from 30 to 120 Hz, the strength of BSR reflection with respect to the water bottom reflection decreases about 40 percent when the RMS amplitude measurements are used and about 50 percent when the peak-trough amplitude measurements are used.

Analysis and Results

Strength of BSR Amplitude

The strength of the BSR amplitude chiefly depends on the impedance contrast, the characteristics at the base of the GHBS, and attenuation of the GHBS. Analyses indicate that the strong BSR amplitudes observed in many low-frequency, multichannel stacked seismic profiles are caused by a marked impedance contrast between GHBS and PGSS (Miller and others, 1991; Dillon and others, 1994; Lee and others, 1994).

The first-order effect on BSR amplitude is the impedance contrast. The BSR reflection coefficient in the Blake Ridge area is on the order of 0.1 to 0.2 (Lee and others, 1994), which was estimated from conventional seismic data with a dominant frequency of 30 Hz. An important question regarding the BSR amplitude has been: Why is it difficult to detect the BSR when a high-frequency source greater than about 200 Hz is used? (Or, similarly, why does the strength of BSR amplitude change significantly with respect to the frequency?) Because the reflection coefficient for the BSR depends on frequency, as demonstrated in figure 1, some of the BSR amplitude variation can be attributed to the velocity dispersion of PGSS, but this frequency-dependent reflection coefficient is not sufficient to fully explain the observed amplitude variation of the BSR.

Analysis and Interpretation of Observed BSR Amplitude

Figure 6 shows a cross plot of the BSR amplitude observed at the dominant frequency of 60 Hz versus that observed at 120 Hz, both of which were calculated using the RMS amplitudes. A dominant frequency of band-pass filtered seismic data was assigned by the method suggested by Lee (1987), whereby the dominant frequency of the band-pass filtered data is about half of the high end of the frequency spectrum. Therefore, the dominant frequencies for the seismic section filtered with 10–60 Hz, 10–120 Hz, and 10–240 Hz are assigned as dominant frequencies of 30 Hz, 60 Hz, and
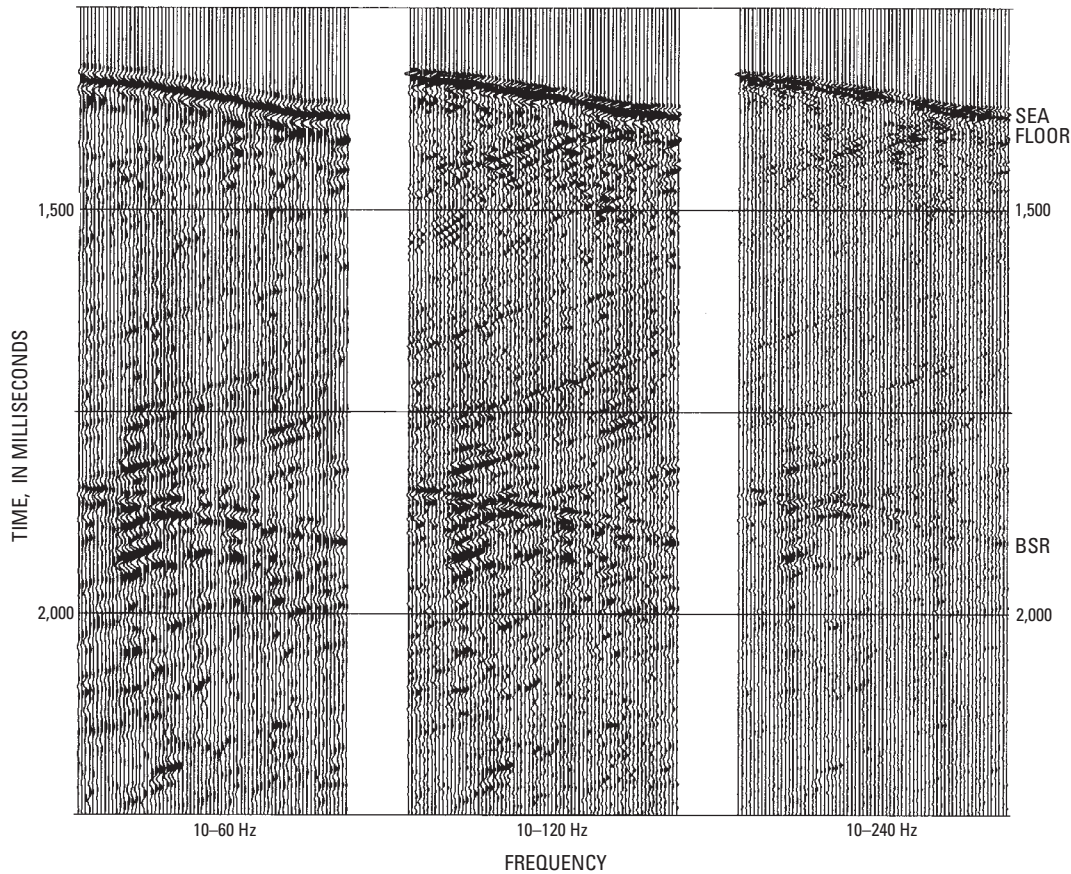
Figure 5. Seismic profiles showing detailed bottom simulating reflections (BSR) acquired at different frequencies in the Blake Ridge area of offshore South Carolina using a single air gun source.

120 Hz, respectively. The cross plot (fig. 6) indicates that the BSR amplitude with respect to the dominant frequency is consistent among the traces and varies by a factor of 2.

The BSR amplitudes shown in figures 7, 8, and 9 are normalized by the BSR amplitude measured at the dominant frequency of 30 Hz. The average normalized BSR amplitudes calculated from the RMS amplitude are 0.73 ± 0.11 and 0.58 ± 0.10 at the dominant frequency of 60 Hz and 120 Hz, respectively. When the peak-trough amplitude is used, they are 0.60 ± 0.15 and 0.48 ± 0.14 at the dominant frequency of 60 Hz and 120 Hz, respectively.

One way to explain the difference of the BSR amplitude with respect to the dominant frequency is by assuming attenuation within GHBS sediments. The result of an attenuation model for the BSR is shown in figure 7A, using the following amplitude relationship:

$$A \propto e^{\left(\frac{-\pi f_p t}{Q}\right)} \tag{4}$$

where

Q is the quality factor

and

t is the two-way travel time.

To compare the amplitude variation with frequency for sediments having different Q and t, a parameter Λ (defined as $\Lambda = t / Q$) is used. Figure 7A shows the predicted normalized reflection amplitude using various values for Λ (5, 2.5, 1.25, 0.5, and 0.25 ms) with measured normalized BSR amplitudes. The amplitudes of BSR analyzed by Chapman and others (2002), also shown in figure 7A for comparison, are normalized by the amplitude at 30 Hz, but, because theirs are estimated from the plot, they are not very accurate. Note that two-way travel time for the Blake Ridge data is ≈ 500 ms and ≈ 250 ms for data analyzed by Chapman and others (2002). If the attenuation model is applicable to the observed BSR amplitude variation, figure 7A indicates that values for Q between 100 and 300 for Blake Ridge amplitude-frequency data and between 50 and 150 for offshore western Canada data fit the amplitude-frequency data quite well.

Another way to explain the difference of the BSR amplitude with respect to the dominant frequency is by assuming a transitional base for the GHBS. The normalized reflection amplitudes predicted from the transitional base having an average velocity of 1.7 km/s are shown in figure 7B, which indicates that a transitional base of about 3 to 8 m would best fit the measured amplitude.

For the above modelings, the frequency-dependent reflection coefficients are not incorporated. Therefore, figure 7 shows only the effects of attenuation and a transitional base on the BSR amplitude in the frequency range of 30 to 200 Hz.
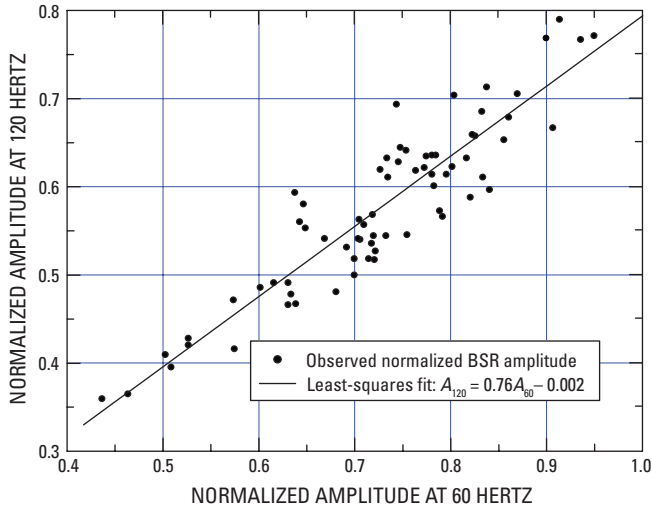
Figure 6. Cross plot of the observed bottom simulating reflection (BSR) amplitude at the dominant frequency of 60 Hz relative to the observed BSR amplitude at 120 Hz. All BSR amplitudes are normalized to 30 Hz and root-mean-square amplitudes were used to compute BSR amplitudes. A linear regression line with a correlation coefficient $r = 0.915$ is shown as a solid line.

Attenuation and Transitional Base

Near the Black Ridge study area, Wood and others (2000) investigated the longitudinal wave (*P*-wave) attenuation from high-frequency single-channel and VSP data using a spectral modeling technique. The estimated *Q* is 90–500, which is only slightly lower than the *Q* values expected for non-gas hydrate-bearing sediments. One of the results from the analysis of single-channel data indicates that the average *Q* for GHBS exceeds 300 (Wood and others, 2000). Brienzo (1992) estimated a *Q* value of 660 at the sea floor to 175 to 750 m below the sea floor in the Monterey, Calif., deep-sea fan for possible GHBS. On the basis of vertical seismic profile data at the Mallik 5L-38 well, Mackenzie Delta, Canada, Lee (2006) estimated attenuation of GHBS to be $Q \approx 150$.

The results shown in figure 7*A* indicate that *Q* values between 100 and 300 for Blake Ridge data and *Q* values between 50 and 150 for offshore western Canada data appear to be close to, or possibly a little lower than, most GHBS analyzed by various investigators. Considering uncertainties associated with estimated attenuation and the amplitude of the BSR, the attenuation is still a feasible mechanism to explain the frequency-dependent BSR amplitudes.
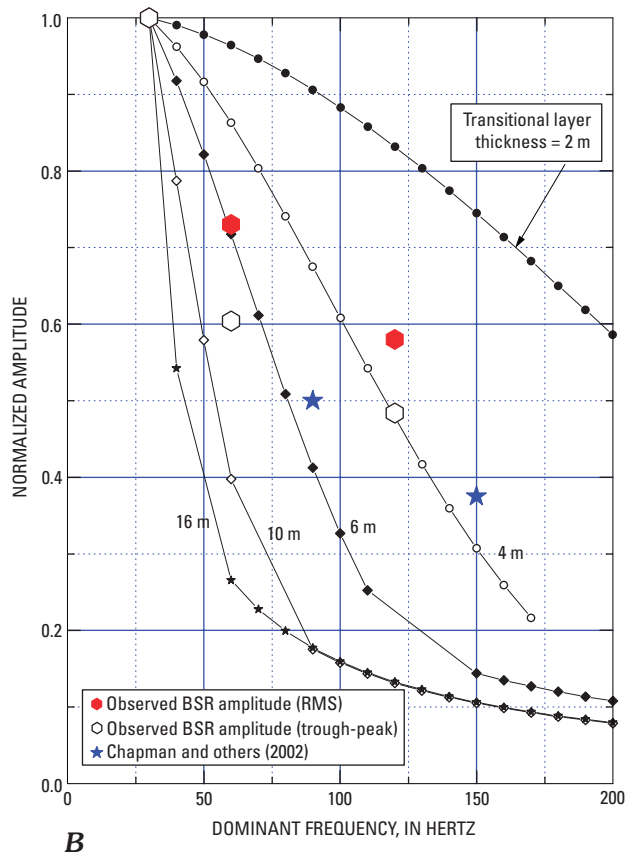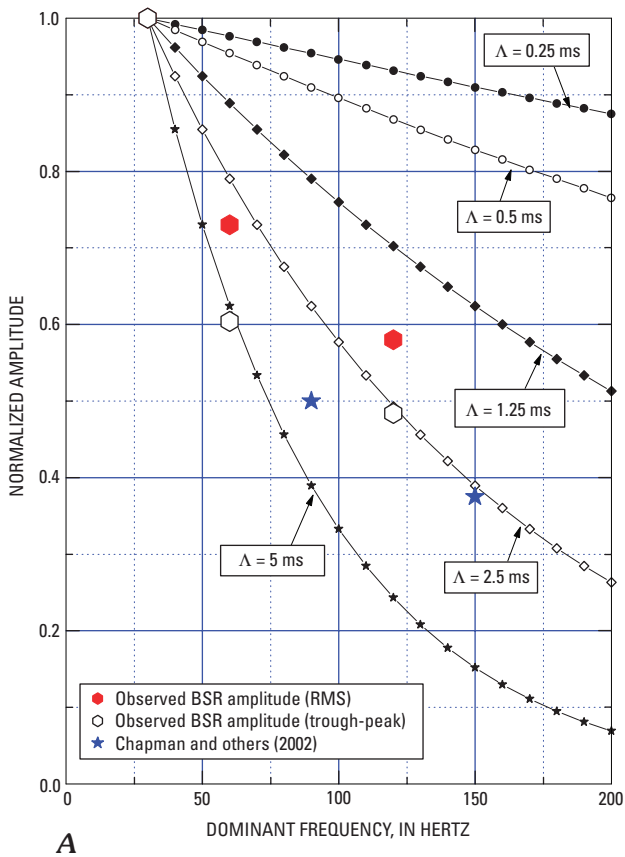
Figure 7. A theoretical bottom simulating reflection (BSR) amplitude reduction without velocity dispersion with respect to the frequency in the range of 20 to 200 Hz. All BSR amplitudes are normalized to the BSR amplitude at 30 Hz. Observed BSR amplitudes (root-mean-square (RMS) amplitude and peak-trough amplitude) and amplitudes analyzed by Chapman and others (2002) are also shown. *A*, attenuation model. Λ is defined as t/Q, where *t* is two-way travel time in milliseconds and *Q* is quality factor; *B*, transitional base model.
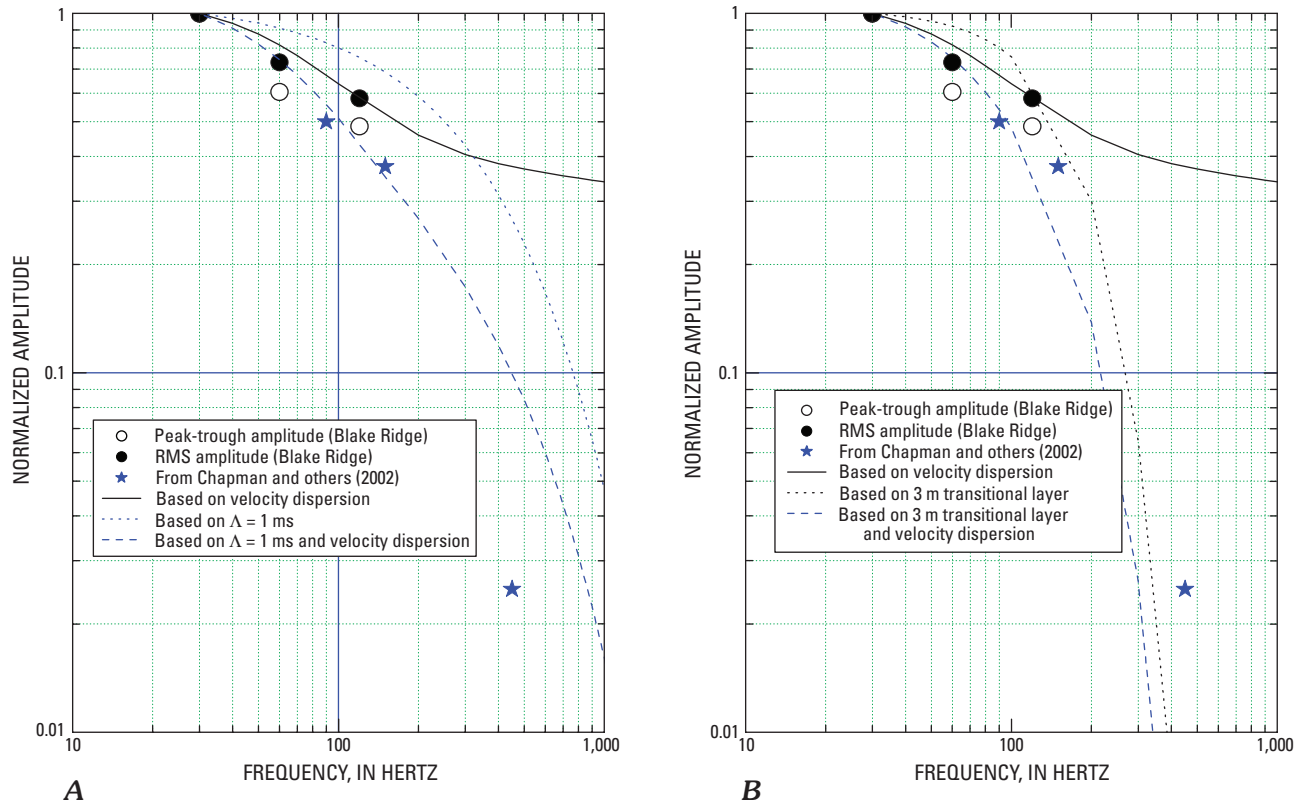
Figure 8. A theoretical bottom simulating reflection (BSR) amplitude reduction with velocity dispersion with respect to the frequency in the range of 20 to 500 Hz. Frequency-dependent reflection coefficient, which is caused by the *P*-wave velocity dispersion of partially gas saturated sediments, is used. All BSR amplitudes are normalized to the BSR amplitude at 30 Hz. Observed BSR amplitudes (root-mean-square (RMS) amplitude and peak-trough amplitude) and amplitudes analyzed by Chapman and others (2002) are also shown. *A*, attenuation model. Λ is defined as *t*/*Q*, where *t* is two-way travel time in milliseconds and *Q* is quality factor; *B*, transitional base model.

Well logs, along with acoustic and electrical resistivity logs, indicate that Ocean Drilling program (ODP) site 995 implies a transitional base with a thickness of about 20 m, but sites 997 and 994 imply a much shorter transitional base (Shipboard Scientific Party, 1996). Travel time inversion from the vertical seismic profiles (Holbrook and others, 1996) implies a large transitional layer, on the order of 50 m, but the seismic resolution is not high enough to determine the accuracy of this assessment. The chloride anomaly at site 994 implies a transitional base about 40 m thick and a much shorter or abrupt base at site 997 (Paull and Matsumoto, 2000), but data are insufficient to warrant a detailed analysis of the base of the GHBS.

Although the accuracy of the transitional base is debatable, it appears that all available information favors some kind of transitional base for GHBS. Therefore, the transitional layer with a thickness of 3–8 m is a reasonable assumption to interpret the behavior of the BSR amplitude with respect to frequency. Chapman and others (2002) also interpreted the amplitude variation of BSR by using a transition layer with 4–8 m thickness at the base of GHBS; however, they used a smooth transitional base rather than the sharp transitional base used in this report. Note that similar transitional layer thicknesses are interpreted for both the Blake Ridge and the offshore western Canada area.

Preferred Model

Although it is not clear which model—transitional base or attenuation—best fits the available data with respect to BSR, the following discussions, interpretations, and conclusions are derived from the present study. Figure 8 shows model results for attenuation and transitional base including the frequency-dependent reflection coefficients in the frequency range between 30 and 500 Hz. The amplitude decay with respect to frequency caused by the frequency-dependent reflection coefficient is much smaller than the measured BSR amplitude variations. The model using Λ = 1 ms (fig. 8*A*), which corresponds to *Q* = 500 for Blake Ridge data and *Q* = 250 for offshore western Canada data, predicts a much higher amplitude for the BSR, although the amplitude decay with respect to frequency is close to the observed decay. The predicted result using both Λ = 1 ms and velocity dispersion agrees well with measured BSR amplitude variation except for the amplitude at 450 Hz. Λ = 1 ms appears to be a reasonable value for frequency less than about 200 Hz, but appears to be high for frequency greater than 400 Hz (fig. 8*A*).

Figure 8*B* shows the model result using both the transitional base and velocity dispersion. Amplitude variation predicted using both a transitional base of 3 m and the velocity

dispersion appears to fit the measured amplitude variation reasonably well except for the amplitude at 450 Hz, where the model overestimates the amplitude decay.

Without considering the amplitude at 450 Hz, the attenuation model appears to best fit the measured amplitude. Figure 8 indicates that $\Lambda = 1$ ms appears to be high and the thickness of 3 m for the transitional layer appears to be too thick for high frequency around 450 Hz.

Figure 9 shows that predicted amplitude variations using both attenuation ($\Lambda = 1$ ms) and a transitional base (thickness of 1 m) agree with measured amplitudes for frequencies less than 500 Hz. The velocity dispersion of PGSS is a well-known phenomenon, and seismic waves are always attenuated. Therefore, the velocity dispersion and attenuation should always be included in the amplitude analysis of BSR. The interpreted transitional base is thin, if both attenuation and velocity dispersion are included in the analysis. Based on the modeling and analysis, attenuation is the most significant effect on the BSR amplitude variation for all frequencies, and a transitional base plays a minor role only at frequencies greater than about 200 Hz.

Constraints on the Model

Model parameters shown in figure 9A ($b = 3$ cm, $\Lambda = 1$ ms, thickness of transition zone of 1 m) are interdependent. The velocity dispersion derived from the White (1975) model depends strongly on the parameter b. If $b = 1$ cm is used in the model, all other parameters should be changed to fit the observation. The P-wave velocity and reflection coefficient using $b = 1$ cm are shown in figure 1 as dotted lines. The velocity dispersion in the seismic frequency band less than 100 Hz is negligible, whereas the velocity dispersion using $b = 3$ cm is substantial (fig. 1). According to White (1975), the velocity dispersion of PGSS is noticeable in the seismic frequency band, so $b = 3$ cm may be the more appropriate parameter to use. The model result using $b = 1$ cm with other parameters adjusted to match the observed amplitude of the BSR, which are $\Lambda = 1.7$ ms and a transition zone thickness of 1.5 m (fig. 9B), indicates that when attenuation is incorporated into the model, the thickness of the transition zone is small.
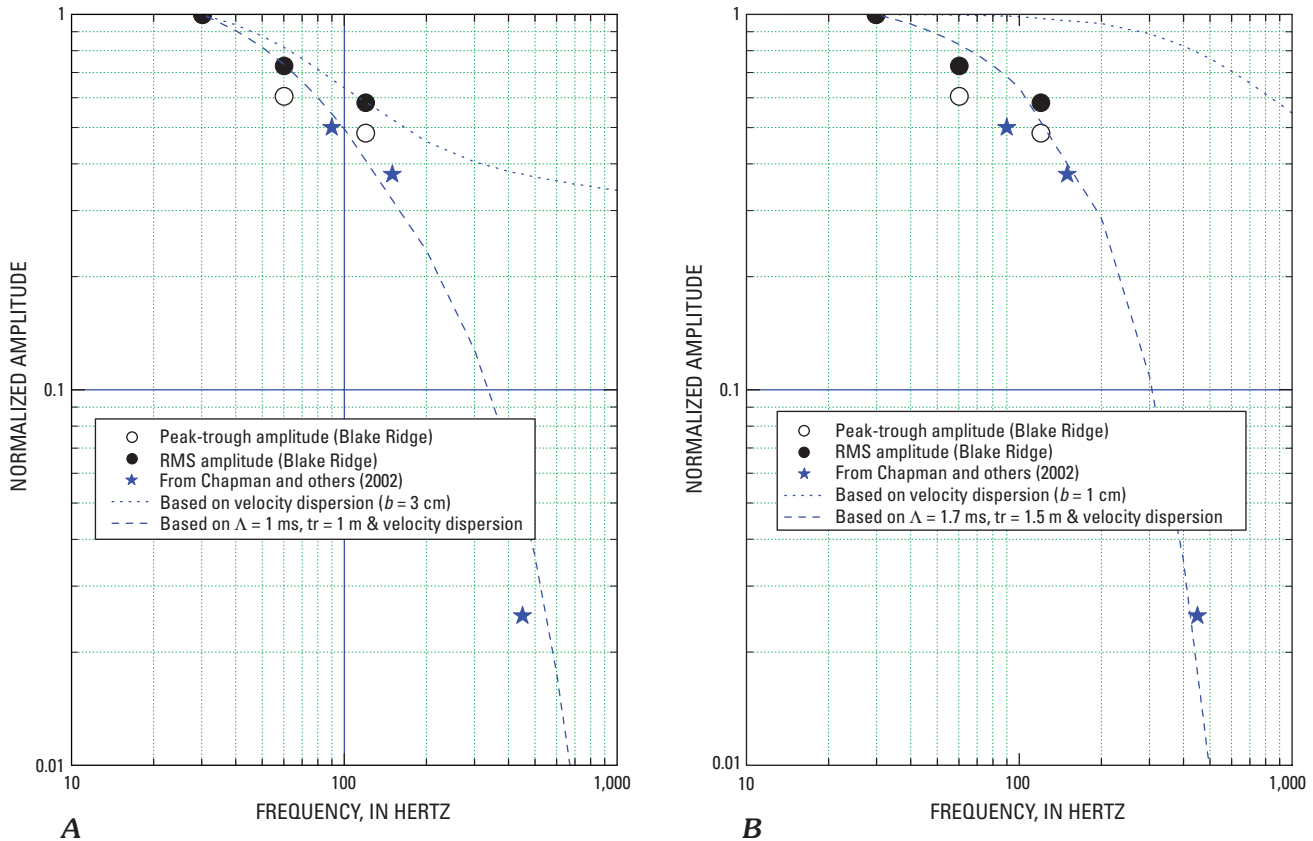
Figure 9.   A theoretical bottom simulating reflection (BSR) amplitude reduction for a preferred model with respect to the frequency in the range of 20 to 500 Hz. Frequency-dependent reflection coefficient, which is caused by the P-wave velocity dispersion of partially gas saturated sediments, is used. All BSR amplitudes are normalized to the BSR amplitude at 30 Hz. Observed BSR amplitudes (root-mean-square (RMS) amplitude and peak-trough amplitude) and amplitudes analyzed by Chapman and others (2002) are also shown. A, using the attenuation with $b = 3$ cm, $\Lambda = 1$ ms, and a transition zone (tr) with a thickness of 1 m; B, using the attenuation with $b = 1$ cm, $\Lambda = 0.6$ ms, and a transition zone with a thickness of 1.5 m. $\Lambda = t/Q$, where t is two-way travel time in milliseconds and Q is quality factor.

The attenuations of $Q = 150$ or $Q = 500$ are plausible values for GHBS in the Blake Ridge and western Canada. However, although velocity dispersion using $b = 1$ cm and $b = 3$ cm can be considered as extreme values, the actual value may be *between* $b = 1$ cm and $b = 3$ cm. Therefore, the thickness of the transition zone using plausible values of Q and b is between 1 m and 1.5 m, which is much less than the thicknesses estimated by Chapman and others (2002).

The transitional characteristics of the base of the GHBS may be related to the amount of gas hydrate saturated in the pore space. If a "recycle model" of methane gas hydrate to enrich the base of GHBS (Paull and others, 1994) is correct, the thickness of the transitional layer should be small, because the highest concentration of hydrate may exist near the phase boundary. However, the phase boundary is dynamic, reflecting effects such as sediment loading, sea level changes, thermal condition, and flux of methane gas. Therefore, the GHBS near the phase boundary are unstable or metastable; dissociation of gas hydrate and (or) formation of gas hydrate occur near the phase boundary. Consequently, the highest gas hydrate concentration may be a little above the phase boundary and a transitional velocity at the base of the GHBS may be possible.

According to Xu and Ruppel (1999), the rate of methane flux at the base of the gas hydrate stability zone controls the thickness of the transition zone. As the flux of methane increases, the transition zone thickness decreases. A sharp boundary is possible if the flux of methane exceeds a critical value. The interpretation of a 1- to 1.5-m thick transition zone for offshore western Canada, where a high average flux rate of 1.3 mm/yr was estimated by Hyndman and others (1993), differs from the 4–8 m of transition zone interpreted by Chapman and others (2002). Although it is unknown if the transition zone thickness of 1 m to 1.5 m is theoretically possible using the average methane flux estimated for offshore western Canada, modeling that includes attenuation restricts the thickness of the transition zone to around 1 m. Because the model parameters are interdependent, the interpretation of the characteristics of BSR amplitude requires caution.

Conclusions

The amplitude reduction of the bottom simulating reflection (BSR) with increasing frequency content is due to the seismic attenuation, the transitional characteristics of the base of gas hydrate-bearing sediments (GHBS), and velocity dispersion of partially gas saturated sediments (PGSS). The amplitude analysis of BSR with respect to the frequency and the model analysis favors the interpretation that attenuation is the dominant effect on the BSR amplitude variation. At Blake Ridge, a model based on Q between 300 and 500 for GHBS and a transitional thickness of $\approx$ 1 to 1.5 m fits well with the observed amplitude variation, whereas Q between 150 and 300 with a transitional thickness of $\approx$ 1 to 1.5 m fits well with

the amplitude measured offshore western Canada. Without incorporating attenuation and velocity dispersion in the analysis, a thicker transitional layer would need to be estimated. Because velocity dispersion and attenuation are inherent to GHBS and PGSS, all BSR amplitude analyses should include these effects regardless of a transitional layer. However, because parameters used to fit the amplitude characteristics of the BSR amplitude are interdependent, a judicious choice of parameters or a restricted range of possible parameters is important.

The BSR amplitude analysis in the present study is limited because only single-channel seismic data acquired with an air gun source in a limited frequency range < 250 Hz are used, although deep-towed seismic data with high frequency by Chapman and others (2002) are incorporated. To better constrain the analysis, multichannel seismic data with a low-frequency source combined with single-channel seismic data with a variety of high-frequency sources shot along the identical line are preferred.

References Cited

Andreassen, Karin, and Berteussen, K.A., 1990, Gas hydrate in the Southern Barents Sea, indicated by a shallow seismic anomaly: First Break, v. 8, p. 235–245.

Brienzo, R.K., 1992, Velocity and attenuation profile in the Monterey deep-sea fan: Journal of Acoustical Society of America, v. 92, p. 2109–2125.

Chapman, N.R., Gettrust, J.F., Walia, R., Hannay, D., Spence, G.D., Wood, W.T., and Hyndman, R.D., 2002, High-resolution, deep-towed, multichannel seismic survey of deep-sea gas hydrates off western Canada: Geophysics, v. 67, p. 1038–1047.

Claypool, G.E., and Kaplan, I.R., 1974, The origin and distribution of methane in marine sediments, *in* Kaplan, I.R., ed., Natural gases in marine sediments: New York, Plenum Press, p. 99–139.

Collett, T.S., 1996, Gas hydrate resources of the United States, *in* Gautier, D.L., Dolton, G.L., Takahashi, K., and Varnes, K.L., eds., 1995 National assessment of United States oil and gas resources on CD-ROM: U.S. Geological Survey Digital Series DDS–30.

Dillon, W.P., Booth, J.S., Paull, C.K., Felhaber, K., Hutchinson, D.R., and Swift, B.A., 1991, Mapping sub-seafloor reservoirs of greenhouse gas—Methane hydrate, *in* Kumar, M., and Maul, G.A., eds., Proceedings of International Symposiums on Marine Positioning: Washington, D.C., Marine Geodesy Committee, Marine Technology Society, p. 545–554.

Dillon, W.P., Lee, M.W., and Coleman, D.F., 1994, Identification of marine hydrates in situ and their distribution off the Atlantic coast of the United States, *in* Sloan, E.D., Jr., Happel, J., and Hnatow, M.A., eds., Natural gas hydrates: Annals of the New York Academy of Sciences, v. 715, p. 346–380.

Gettrust, J.F., Wood, W., Lindwall, D., Chapman, R., Walia, D., Spence, G., Macdonald, R., and Hyndman, R.D., 1999, New seismic study of deep sea gas hydrates results in greatly improved resolution: Eos, September 12, p. 439–440.

Guerin, Gilles, Goldberg, D., and Melster, A., 1999, Characterization of in situ elastic properties of gas hydrate-bearing sediments on the Blake Ridge: Journal of Geophysical Research, v. 104, p. 17782–17795.

Holbrook, W.S., Hoskins, H., Wood, W.T., Stephen, R.A., Lizzarralde, D., and the Leg 164 Science Party, 1996, Methane gas-hydrate and free gas on the Blake Ridge from vertical seismic profiling: Science, v. 273, p. 1840–1843.

Hyndman, R.D., and Davis, E.E., 1992, A mechanism of formation of methane hydrate and seafloor bottom-simulating reflections by vertical fluid expulsion: Journal of Geophysical Research, v. 97, p. 7025–7041.

Hyndman, R.D., and Spencer, G.D., 1992, A seismic study of methane hydrate marine bottom simulating reflectors: Journal of Geophysical Research, v. 97, p. 6683–6698.

Hyndman, R.D., Wang, K., Yuan, T., and Spence, G.D., 1993, Tectonic thickening, fluid expulsion and the thermal regime of subduction zone accretionary prism—The Cascadian margin off Vancouver Island: Journal of Geophysical Research, v. 98, p. 399–419.

Justice, J.H., and Zuba, C., 1986, Transition zone reflections and permafrost: Geophysics, v. 51, p. 1075–1086.

Kvenvolden, K.A., 1988, Methane hydrate—A major reservoir of carbon in shallow geosphere: Chemical Geology, v. 71, p. 41–71.

Lee, M.W., 1987, Particle displacements on the wall of a borehole from incident plane waves: Geophysics, v. 52, p. 1290–1296.

Lee, M.W., 2002, Modified Biot-Gassmann theory for calculating elastic velocities for unconsolidated and consolidated sediments: Marine Geophysical Researches, v. 23, p. 403–412.

Lee, M.W., 2006, Is amplitude loss of sonic waveforms due to intrinsic attenuation or source coupling of the medium?: U.S. Geological Survey Scientific Investigations Report 2006–5120, 13 p.

Lee, M.W., Hutchinson, D.R., Agena, W.F., Dillon, W.P., Miller, J.J., and Swift, B.A., 1994, Seismic character of gas hydrates on the Southeastern U.S. Continental margin: Marine Geophysical Researches, v. 16, p. 163–184.

Markl, R.G., Bryan, G.M., and Ewing, J.I., 1970, Structure of the Blake-Bahama Outer Ridge: Journal of Geophysical Research, v. 75, p. 4539–4555.

Miller, J.J., Lee, M.W., and von Huene, R., 1991, An analysis of a reflection from the base of a gas hydrate zone offshore Peru: American Association of Petroleum Geologists Bulletin, v. 75, p. 910–924.

Paull, C.K., and Matsumoto, R., 2000, Leg 164 overview, *in* Paull, C.K., Matsumoto, R., Wallace, P.J., and Dillon, W.P., eds., Proceedings of the Ocean Drilling Program, Scientific Results: College Station, Tex., v. 164, p. 3–10.

Paull, C.K., Ussler, W. III, and Borowski, W.S., 1994, Sources of biogenic methane to form marine gas hydrates, *in* Sloan, E.D., Jr., Happel, J., and Hnatow, M.A., eds., Natural gas hydrates: Annals of the New York Academy of Sciences, v. 715, p. 346–380.

Paull, C.K., Ussler, W. III, and Dillon, W.P., 1991, Is the extent of glaciation limited by marine gas-hydrates?: Geophysical Research Letters, v. 18, p. 432–434.

Shipboard Scientific Party, 1996, Sites 994, 995, and 997 (Leg 164), 1996, *in* Paull, C.K., Matsumoto, R., Wallace, P.J., and others, eds., Proceedings of the Ocean Drilling Program, Initial Reports: College Station, Tex., v. 164, p. 99–623.

Shipley, T.H., Houston, M.H., Buffler, R.T., Shaub, F.J., McMilen, K.J., Ladd, J.W., and Worzel, J.L., 1979, Seismic evidence for widespread possible gas hydrate horizons on continental slopes and rises: American Association of Petroleum Geologists Bulletin, v. 61, p. 698–707.

White, J.E., 1975, Computed seismic speeds and attenuation in rocks with partial gas saturation: Geophysics, v. 40, p. 224–232.

Wood, W.T., Holbrook, W.S., and Hostkins, H., 2000, In situ measurements of *p*-wave attenuation in the methane hydrate- and gas-bearing sediments of the Blake Ridge, *in* Paull, C.K., Matsumoto, R., Wallace, P.J., and Dillon, W.P., eds., Proceedings of the Ocean Drilling Program, Scientific Results: College Station, Tex., v. 164, p. 265–272.

Xu, Wenyue, and Ruppel, C., 1999, Predicting the occurrence, distribution and evolution of methane gas hydrate in porous marine sediments: Journal of Geophysical Research, v. 104, p. 5081–5095.

Appendix.   Reflections from Transition Zones

The amplitude from a transitional base is calculated using the Ricker wavelet. The Ricker wavelet $r(t)$ is given by the following formula

$$r(t) = (1 - 2\alpha t^2)e^{-\alpha t^2} \tag{5}$$

with $\alpha = \pi^2 f_p^2$, where f_p is the dominant frequency of the Ricker wavelet in hertz.

Defining $G(t) = e^{-\alpha t^2}$, then

$$r(t) = -\frac{d^2 G}{dt^2}/(2\alpha) \text{ and } G'(t) = -2\alpha t G(t) \tag{6}$$

The reflected wavefield $(S(t))$ from the first-order transitional boundary is given by Justice and Zuba (1986):

$$S(t) = \frac{\ln(V_1/V_0)}{2T} \int r(\tau) d\tau \tag{7}$$

where

V_0 is the velocity at the top of the transition zone,
V_1 is the velocity at the bottom of the transition zone,

and

T is the width of the transition zone in two-way time.

The integration shown in equation 7 can be written as follows using equation 6:

$$\int_t^{t+T} r(\tau) d\tau = (t+T)G(t+T) - tG(t) \tag{8}$$

Therefore, the reflection waveform from the transition zone is given by

$$S(t) = \frac{\ln(V_1/V_0)}{2T}\left[(t+T)G(t+T) - tG(t)\right] \tag{9}$$

It is instructive to see the waveform in the following limit

$$\lim_{T\to 0} S(t) = \lim_{T\to 0} \frac{c\left[\ (t+T)G(t+T) - tG(t)\ \right]}{T} \approx c\frac{d(tG)}{dt} = cr(t) \tag{10}$$

where c is a constant given by $ln\ (V_1/V_0)/2$, which is the reflectivity of the transition boundary. Equation 10 indicates that, as the thickness of the transitional layer approaches zero, the waveform of the reflection approaches the input waveform and its magnitude is proportional to the reflection coefficient. When T is much greater than the period of the input, two reflections, one with $(t+T)G(t+T)$ and the other with $tG(t)$, are separated in time, so the waveform is proportional to $tG(t)$. Because $tG(t)$ is proportional to $G'(t)$, it can be shown, using equation 6, that the reflected waveform from a thick transitional layer is the integrated waveform of the input.

The extremes of the reflection amplitude are at $dS(t)/dt = 0$, which is

$$\frac{dS}{dt} = 0 = G(t+T) + (t+T)G'(t+T) - G(t) - tG'(t). \tag{11}$$

Case 1.   The duration of the wavelet is longer than or similar to the transitional layer thickness. In this case, the extreme occurs at $t = -T/2$ and the extreme is given by

$$A_{max} = cG(T/2) = ce^{-\alpha(T/2)^2} \tag{12}$$

Case 2.   The duration of the input wavelet is much shorter than the transition thickness. In this case, there is no interference between the top and bottom reflections. Therefore, two extreme amplitude points exist and the extreme condition is $G(t) + tG'(t) = 0$ or $G(t + T) + (t + T)G'(t + T) = 0$. The extreme point occurs at $t = \sqrt{1/(2\alpha)}$ or $t = \sqrt{1/(2\alpha)} - T$. The extreme amplitude at these points is given by

$$A_{max} = \frac{c}{T}\sqrt{\frac{1}{2\alpha}}e^{-1/2} \tag{13}$$

Case 3.   The duration of the input wavelet is between case 1 and case 2. There is no simple analytic solution.

The Fourier amplitude spectrum of the Ricker wavelet, $R(\omega)$, is given by

$$R(\omega) = \frac{\omega^2 G(\omega)}{2\alpha} = \frac{4\pi\omega^2}{\omega_p^2}e^{-\omega^2/\omega_p^2} \tag{14}$$

where

ω_P is the angular dominant frequency of the Ricker wavelet.

The amplitude spectrum of the reflection from a transition zone can be written, using equations 8 and 14 and from Justice and Zuba (1986),

$$S(\omega) = \frac{c\omega^2 \sin(\omega T/2)}{(\omega T/2)}e^{-\omega^2/\omega_p^2} \tag{15}$$

Equation 15 indicates that when T approaches zero, the spectrum of the reflection is proportional to the input wavelet. On the other hand, when T becomes larger, the amplitude spectrum approaches the spectrum of the integrated Ricker wavelet. Therefore,

$$S(\omega) \propto \omega e^{-\omega^2/\omega_p^2} \tag{16}$$

The maximum of equation 16 is at $\omega = \omega_p/\sqrt{2}$. This implies that the amplitude spectrum of a reflection from a thick transitional layer shifts towards a lower frequency and approaches about 70 percent of the dominant input frequency.

Figure 10*A* shows the peak amplitudes of transition zone reflections with respect to the transition zone thicknesses and the dominant frequency of the Ricker wavelet, and figure 10*B* shows the actual waveforms. The reference peak amplitude is the reflection amplitude from the discontinuous (sharp) boundary, which is equivalent to the transition zone thickness of zero. When λ, which is defined as the ratio of the transition zone thickness in two-way time (T) to the dominant period of the input wavelet ($1/f_p$), is less than about 0.8 (Region I), the peak amplitude is given by equation 12 and drops off rapidly with respect to λ: its value is about –12 db at $\lambda = 0.8$. In this region, the reflected waveform is close to the input waveform except that the dominant frequency of reflection shifts to the lower frequency as λ increases.

In Region II, where λ is between 0.8 and 1.1, there is no simple solution for the peak amplitudes or the waveforms. The peak amplitude in this zone varies between about –12 db and –17 db compared to the reference amplitude, and its waveform varies according to the amount of interference between the reflection from the top and bottom of the transitional layer.

In Region III, where λ is greater than 1.1, the waveform is similar to the integrated input waveform, and the peak amplitude is given by equation 13 and decays slowly with λ.
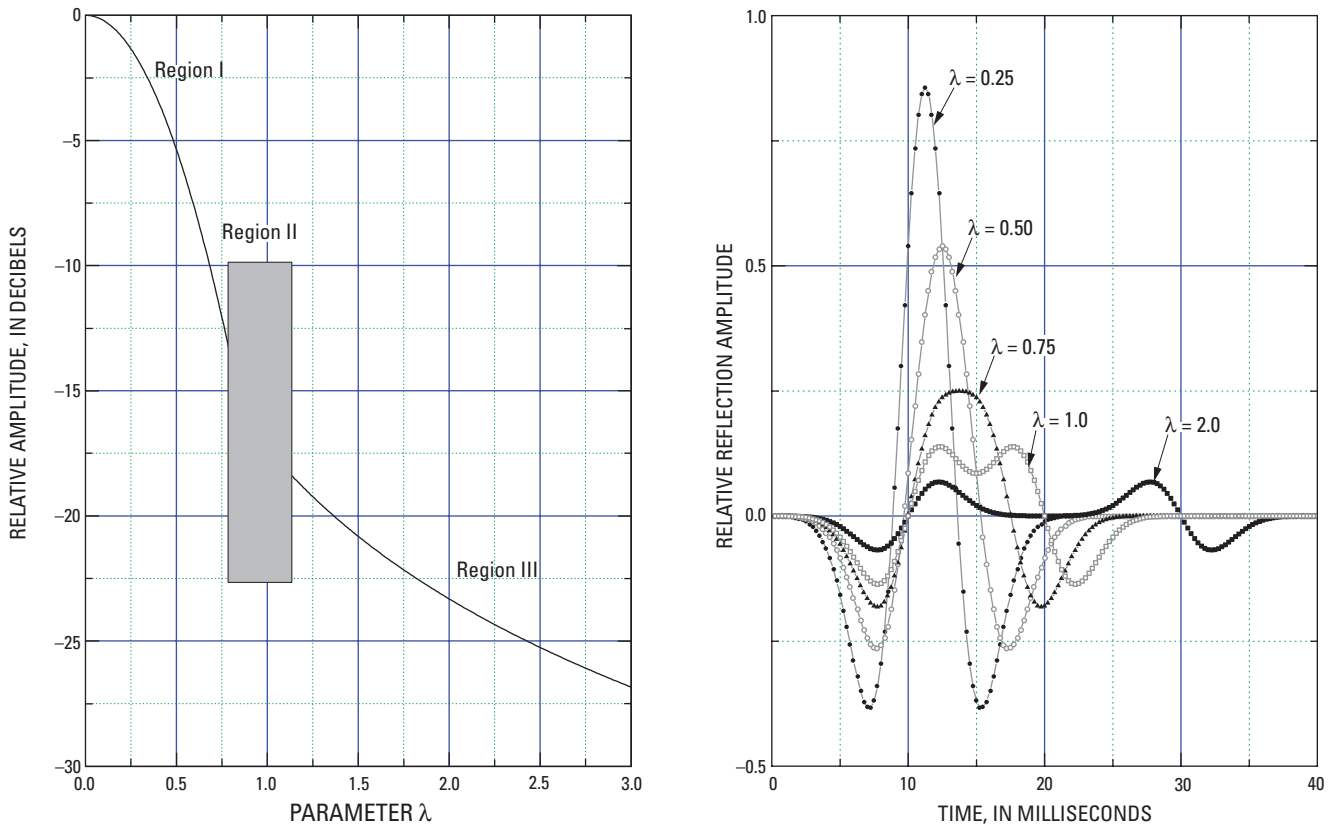
Figure 10. Relationships between reflection amplitude and transitional layer thickness. *A*, relationship between maximum reflection amplitude and transition zone thickness; *B*, reflection waveforms from transition zones. Parameter λ is the ratio of transition zone thickness in two-way time to the period of the dominant symmetrical Ricker wavelet.